

Article

Experimental Study of Surface Damage of Stainless Steel Subjected to Cavitation Collapse in Aqueous Environment

Lei Liu ^{*}, Lei Zhang, Chuanhui Huang, Huafeng Guo, Jiayang Man and Ping Yu 

School of Mechanical and Electrical Engineering, Xuzhou University of Technology, Xuzhou 221000, China; triple-stone@foxmail.com (L.Z.); huangch2008@xzit.edu.cn (C.H.); ghfmaster@163.com (H.G.); yuping050201@163.com (P.Y.)

* Correspondence: leiliu86@sina.cn; Tel.: +86-13914885071

Abstract: With the aim of understanding cavitation damage of stainless steel under the effect of cavitation collapse in an aqueous environment, morphology, phase, chemical state, electrochemical, and other properties after cavitation and erosion are methodically examined. The obtained results indicate that the addition of metal ions in pure water strengthens the dynamic effect of cavitation collapse. When the cavitation collapses, it is capable of releasing a high temperature and transferring it to the surface of the stainless steel in a short time. Then, through the rapid cooling of the pure water environment, the martensitic structure is generated, but the presence of a massive amount of metal ions leads to a decrease in the speed of heat conduction and absorption of some heat. After the collapse of the bubble, the passivation film on the surface of the stainless steel incorporates into the creation of initial micropores. A concentration difference and a growth of the current density at the bottom of the hole, as well as a reduction in the pH value are detectable. Compared with pure water, 3.5% NaCl solution contains more free ions and its local current density is higher, so its corrosion resistance is worse.

Keywords: average water; stainless steel; cavitation; surface damage; model



Citation: Liu, L.; Zhang, L.; Huang, C.; Guo, H.; Man, J.; Yu, P. Experimental Study of Surface Damage of Stainless Steel Subjected to Cavitation Collapse in Aqueous Environment. *Coatings* **2023**, *13*, 1356. <https://doi.org/10.3390/coatings13081356>

Academic Editors: Luigi Calabrese and Ludmila B. Boinovich

Received: 5 April 2023

Revised: 27 July 2023

Accepted: 31 July 2023

Published: 2 August 2023



Copyright: © 2023 by the authors. Licensee MDPI, Basel, Switzerland. This article is an open access article distributed under the terms and conditions of the Creative Commons Attribution (CC BY) license (<https://creativecommons.org/licenses/by/4.0/>).

1. Introduction

Cavitation is a common form of damage in engineering machinery, marine equipment, and other fields. Meanwhile, cavitation of the pure water environment is a more severe threat [1], which seriously limits the development and application of pure water environment engineering equipment. Cavitation damage of valve components is substantially influenced by many factors, such as the energy release of cavitation collapse [2,3], which is associated with dynamic and thermodynamic processes. The cavitation bubble generally occurs near the downstream of the hydraulic valve throttle. The expansion of the downstream low-pressure area leads to the growth and development of bubbles and then their collapse [4]. The bubbles collapse to a minimum volume [5] in the far field and release high-intensity pressure pulses [6,7], and form a shock wave of high levels of pressure and speed. The shock wave acts on the metal surface and causes local plastic deformation of the surface [8] and the collapsed bubbles do not disappear. When they collapse to a minimum volume and flow again in the locally low-pressure region, they will rapidly rebound and create a very strong secondary shock wave [9]. During bubble regeneration and rebound, two observable rebounds occur; however, the size of the rebound gradually decreases [10]. The pits formed by cavitation collapse are symmetric cones [11] that successively cause surface hardening, plastic deformation, erosion, and cracking [12], expand in the depth direction, and merge along the horizontal direction [13]. In the final stage of bubble collapse, the thermal effect plays a very important role. In the process of the rapid collapse of the bubble, a very high local and transient temperature appears in the bubble [3] and the resulting heat at the moment of collapse spreads to the surrounding fluid, which has

a vital effect on the fluid and solid wall outside the bubble. Qin et al. [14] developed a bubble heat transfer model accounting for the effects of heat conduction and radiation, and then examined the collapse and rebound process of bubbles when they move along the flow. Yang et al. [15] explored the thermodynamic effect of bubble collapse by employing the lattice Boltzmann method and appropriately characterized the temperature evolution law of the gas–liquid phase. Under the action of the fluid’s pressure and velocity, the heat generated by the high temperature during bubble collapse is transferred to the wall in the direction of the jet [16]. The material properties of the fluid environment commonly determine the degree of influence of the thermal effect of bubble collapse [17]. It can be seen that cavitation is a type of damage caused by energy release after cavitation collapse. The release of energy includes two forms, heat and force, but previous studies have not provided specific explanations on the impact of thermal coupling on cavitation. Therefore, aiming at cavitation in a pure water medium, this paper aims to examine the dynamics and thermodynamic coupling effect produced by cavitation collapse, and a 3.5% NaCl solution is utilized for a comparative study.

2. Cavitation Model and Analysis

Cavitation models were developed for pure water and 3.5% NaCl solution, respectively, as demonstrated in Figure 1.

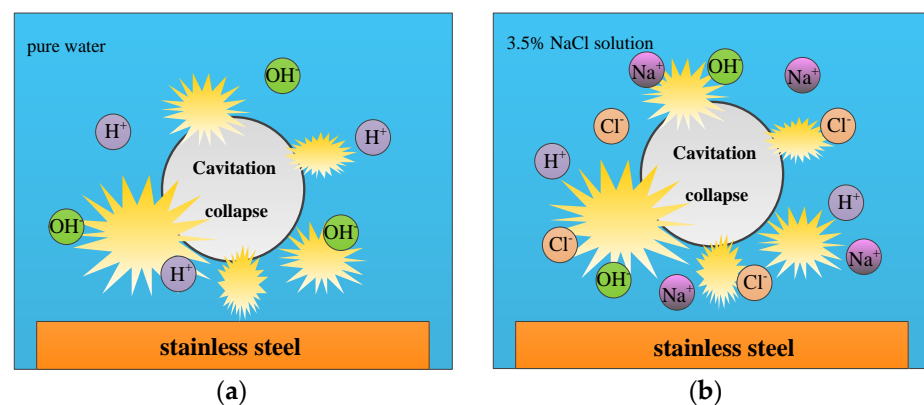


Figure 1. Two cavitation models: (a) pure water cavitation model and (b) cavitation model of 3.5% NaCl solution.

Model A: cavitation model of pure water. The pure water contains very little H^+ and OH^- ions (about 1×10^{-7} mol/L), dynamics, and thermodynamic energy of bubble collapse all act on the stainless-steel surface. The influence of cavitation collapse is somehow equivalent to the water hammer effect, and because the release of collapse heat will be accompanied by alterations of the chemical state of the elements; finally, due to the long action time, the shape of the surface will be destroyed by cavitation.

Model B: cavitation model of 3.5% NaCl solution. In addition to H^+ and OH^- ions, the water also contains a large number of Na^+ and Cl^- ions. The dynamics and thermodynamic energy of cavitation collapse are partly absorbed by ions and cannot fully act on the surface of stainless steel. Therefore, its damage form is mostly dynamic damage, and the effect of thermodynamic damage, also in the early stages of cavitation damage, is relatively low.

3. Experimental Approach

The ultrasonic cavitation testing machine (Nanjing Shunliu SLQS1000, Nanjing, China) was utilized to simulate the cavitation damage test of a medium water valve. The experimental device has been presented in Figure 2. The test parameters are as follows: ultrasonic power, 500 W; 20 kHz ultrasonic frequency; Horn diameter $\Phi 15$ mm, 1 mm from the sample surface. The temperature was set as 20 °C. The stainless-steel sample should be polished to

8000 mesh before testing; the dimensions are 20 mm × 20 mm × 0.5 mm. After the test, the sample was cleaned, dried with cold air, and then sealed.

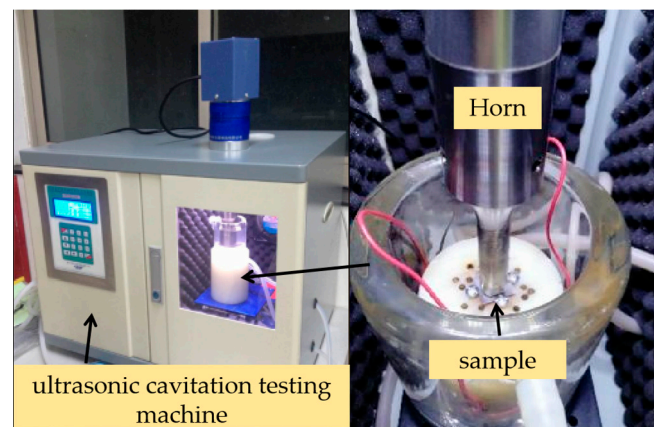


Figure 2. Photos of the experimental devices.

Experimental process: Cavitation tests were performed in pure water and 3.5% NaCl solution for 24 and 48 h, and then changes in surface morphology, phase composition, chemical state, and other parameters were carefully investigated using a scanning electron microscope (FEI Inspect F50, FEI Company, Hillsboro, USA), an X-ray diffraction (Bruker D8 advance, Bruker Company, Karlsruhe, Germany), an X-ray photoelectron spectroscopy (Thermo EscaLab 250Xi, Thermo Fisher Scientific Company, Waltham, Massachusetts, USA), and an electrochemical workstation (Shanghai Chenhua CHI1030B, Shanghai, China).

4. Results and Discussion

The SEM diagram of the surface after the cavitation of the aqueous environment (Figure 3) indicates that the size of the surface particles caused by the cavitation of 3.5% NaCl solution is smaller than that produced in the presence of the pure water cavitation. This fact reveals that the addition of metal Na^+ in pure water strengthens the dynamic effect of the cavitation collapse. Compared to water hammer performance in pure water cavitation, the hardness of metal ions is much higher than that of water. Therefore, the stronger the dynamic action caused by metal ions, the more severe the cavitation damage.

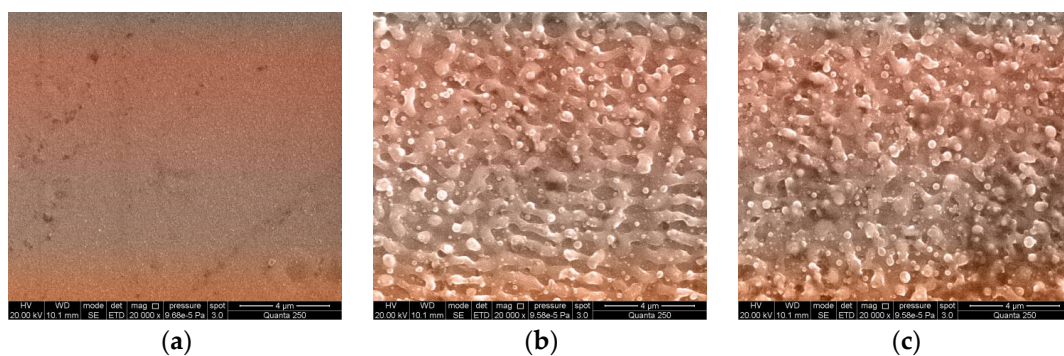


Figure 3. Levels of cavitation of the water environment: (a) original stainless-steel sample, (b) cavitation of pure water for 48 h, and (c) cavitation of 3.5% NaCl solution for 48 h.

The components of the cavitation surface products were analyzed using XRD, as shown in Figure 4. The results demonstrate that the stainless-steel samples in five groups have three main peaks at 44.54° , 51.6° , and 75.44° , respectively, which are austenite 111, 200, and 220 structure, and a weak martensitic 110 structure.

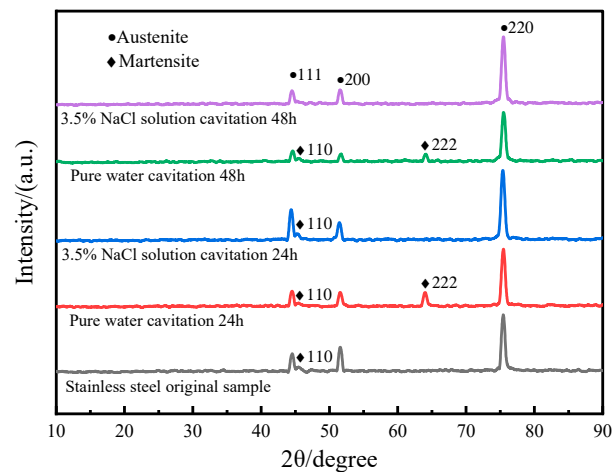


Figure 4. XRD surface damage due to the cavity.

In addition, there is a peak of 64.02° in the test samples under pure water cavitation for 24 and 48 h, which represents a typical structure of martensite 222. The major reason is that austenite can be transformed into martensite after high temperatures, which indicates that cavitation collapse can release a high amount of heat and transfer it to the surface of stainless steel in a short time, and the rapid cooling of the pure water medium leads to the martensite structure. Nevertheless, in the cavitation condition of 3.5% NaCl solution, due to the presence of ions in the solution, the speed of heat conduction decreases and part of the heat is absorbed by the ions, so the heat transfer on the stainless steel surface would be inadequate; thereby, 222 martensite is not produced. In order to further analyze the element changes on the cavitation stainless steel surface, the XPS analysis and peak fitting were performed on the sample surface, as demonstrated in Figure 5.

The plotted results in Figure 5a indicate that the XPS spectrum of O1s under the action of pure water cavitation is substantially different from other samples since the O content is remarkably lessened and the peak position is larger. Figure 5b displays that the fitting peaks at the binding energies of 707.1 and 713.8 eV of the original stainless-steel sample are associated with the simple substance Fe, while the binding energy of 710.5 eV is pertinent to the compound of Fe^{3+} [18,19], namely Fe_2O_3 . The demonstrated graphs in Figure 5c show that the fitting peak at the binding energy of 706.7 eV is associated with the simple substance Fe, whereas the binding energy of 709.6 eV corresponds to the compound of Fe^{2+} , i.e., FeO, and the binding energy of 711.6 eV is pertinent to the compound of Fe^{3+} , which is Fe_2O_3 . The depicted results in Figure 5d are provided for the case of 3.5% NaCl solution cavitation 24 h. As can be seen, the fitting peak at the binding energy of 707.5 eV is associated with the simple substance Fe, the binding energy of 710.9 eV is pertinent to the compound of Fe^{3+} (i.e., Fe_2O_3), the binding energy of 713.1 eV corresponds to the compound of Fe^{2+} (i.e., FeCl_2), and, finally, the binding energy of 723.4 eV is associated with the compound of Fe^{2+} and Fe^{3+} (i.e., Fe_3O_4). The graphs presented in Figure 5e reveal that the fitting peak at the binding energy of 708.7 eV is pertinent to the simple substance Fe, whereas the binding energy of 711.8 and 714.2 eV is associated with the compound of Fe^{3+} , namely $\text{Fe}(\text{OH})_3$ and $\text{Fe}_2(\text{SO}_4)_3$, after the pure water cavitation for 48 h. The demonstrated results in Figure 5f indicate that after cavitation of 3.5% NaCl solution for 48 h, the fitting peak at the binding energy of 707.5 eV corresponds to the simple substance Fe, while the binding energy of 710.7 eV and 714.2 eV are pertinent to the compound of Fe^{3+} , namely FeCl_3 and $\text{Fe}_2(\text{SO}_4)_3$, respectively. It is proved that based on the cavitation collapse shock and heat transfer, an electrochemical reaction also takes place. For the sake of examining the electrochemical effect of the cavitation damage on stainless-steel materials, the polarization and impedance curves are analyzed through the CHI electrochemical workstation, as presented in Figure 6.

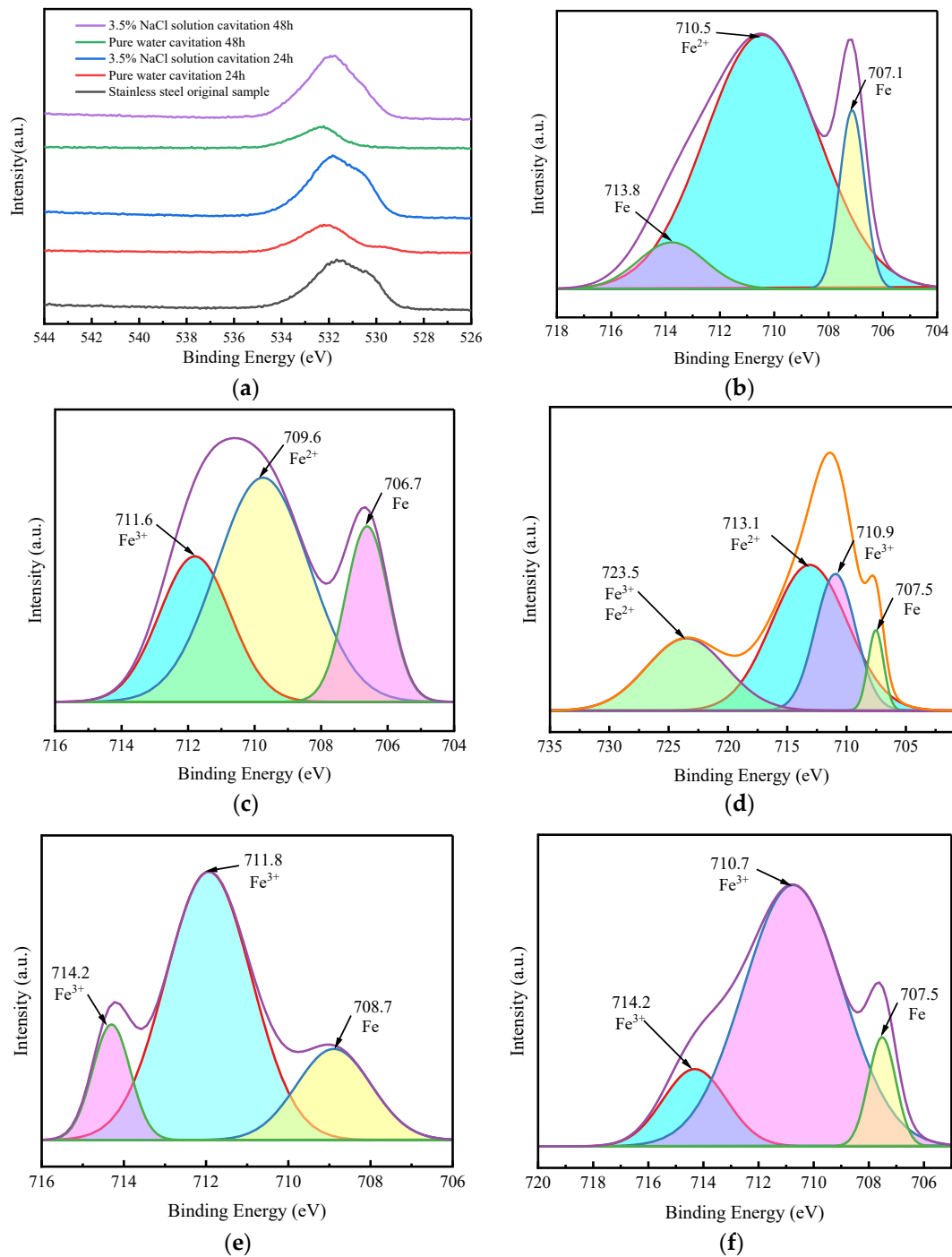


Figure 5. XPS spectrum of stainless-steel sample under various cavitation conditions: (a) XPS narrow spectrum of O1s, (b) original Fe2p sample, (c) pure water cavitation 24 h Fe2p, (d) 3.5% NaCl solution cavitation 24 h Fe2p, (e) pure water cavitation 48 h Fe2p, and (f) 3.5% NaCl solution cavitation 48 h Fe2p.

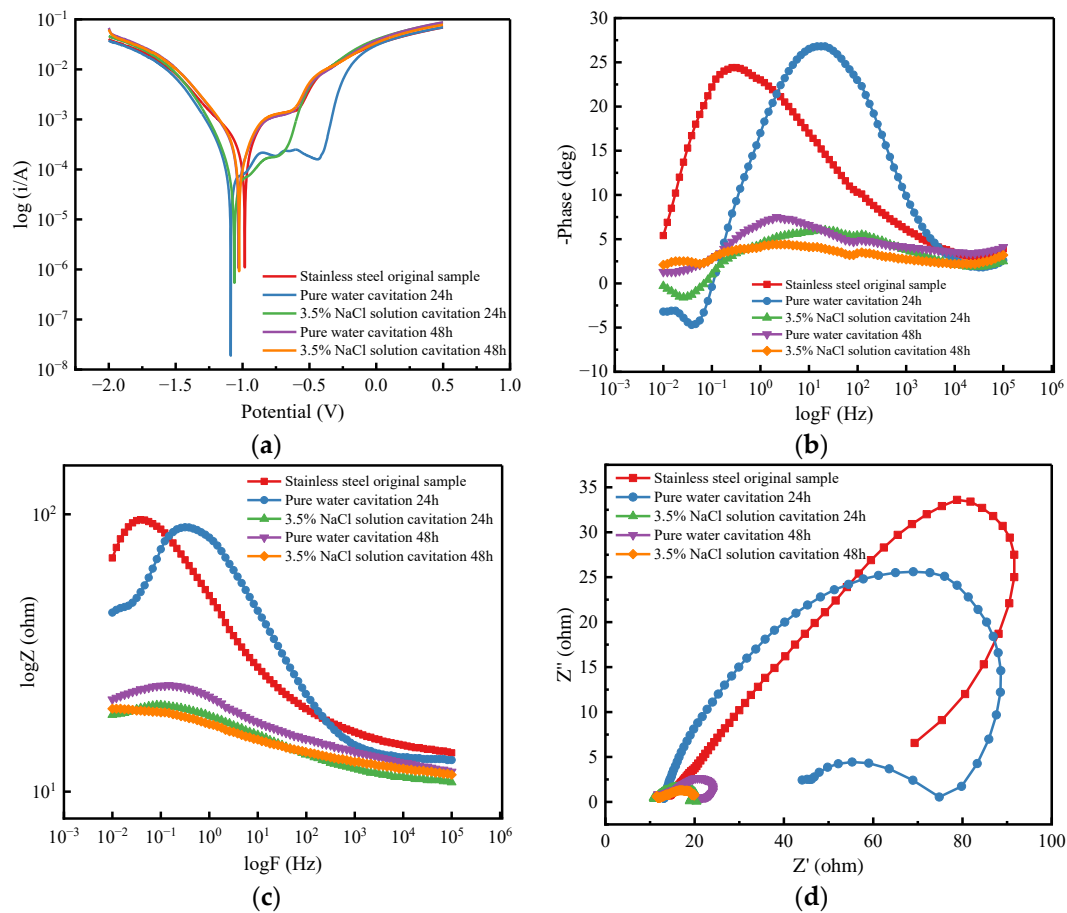
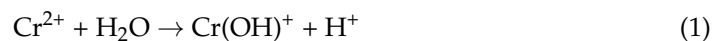


Figure 6. Polarization and impedance curves under various cavitation conditions: (a) polarization curve and (b–d) polarization curve.

After pure water cavitation, the passivation film on the surface of 304 stainless steel is relatively fragile compared to its surroundings, resulting in a high current density in the available region. At this time, the corrosion anions in the corrosion solution near the metal cations are dissociated and combined with them to form a complex, and the passivation film is destroyed in such a case. At the same time, the cavitation ion stainless-steel sample, due to the influence of the two-phase flow caused by the collapse of cavitation on the matrix surface, leads to the destruction of the interface of the matrix phase and the formation of micropores [20]. The micropores are lower than the surrounding matrix area, and the solution is difficult to disperse inside and outside the hole, causing a difference in concentration inside and outside the hole. Such a fact leads to the lessening of its self-corrosion potential and hydrolysis process of Cr^{2+} :



On the other hand, the increase in H^+ content after the electrochemical reaction results in a decrease in the pH value of 3.5% NaCl solution after cavitation. This issue is essentially attributed to two factors: the acidic corrosion solution continues to reduce the stability of the passive film, thereby accelerating the degradation of the passive film, while also leading to the growth of the current density at the bottom of the pores, hence contributes to the lessening of the pH value. The surface defects of stainless steel after cavitation in the 3.5% NaCl solution essentially consist of tiny pores and cracks. The pores are able to promote the formation and expansion of corrosion pits, and pores and cracks effectively influence the corrosion resistance of the stainless steel. The corrosion potential of the sample after cavitation of pure water is lower than that of the stainless-steel sample after cavitation in

the presence of 3.5% NaCl solution. As the cavitation time increases, the corresponding passivation zone of the sample gradually disappears. The electrochemical corrosion current and potential of various samples are given in Table 1.

Table 1. Electrochemical corrosion currents and potentials of different samples subjected to cavitation.

Sample	Corrosion Potential (V)	Current Density (A/cm ²)	Pitting Potential (V)
Pure Water Cavitation 24 h	−1.088	2.118×10^{-5}	−0.428
3.5% NaCl Solution Cavitation 24 h	−1.061	1.908×10^{-5}	−0.713
Pure Water Cavitation 48 h	−1.029	3.700×10^{-5}	−0.62
3.5% NaCl Solution Cavitation 48 h	−1.026	3.476×10^{-5}	−0.616
Stainless-steel Original Sample	−0.983	5.357×10^{-5}	−0.585

By combining the provided results in Table 1 and those of Figure 6b–d, it can be seen that the corrosion resistance of the original sample and the sample after pure water cavitation is superior to the sample after cavitation by 3.5% NaCl solution from the impedance spectrum. The corresponding capacitance arc radius of various samples follows the following order: the original sample of stainless steel > the sample after pure water cavitation for 24 h > the sample after pure water cavitation for 48 h > the sample after 3.5% NaCl solution cavitation for 24 h > the sample after 3.5% NaCl solution cavitation for 48 h.

5. Conclusions

The addition of metal ions in pure water strengthens the dynamic effect of cavitation collapse. Actually, compared to the water-hammer effect in pure water cavitation, the hardness of metal ions is much higher than water, hence, the impacts of the dynamic are much stronger, and, thereby, the cavitation damage would be more intense.

When the cavitation collapses, it can release a high amount of heat and transfer it to the surface of the stainless steel in a short time. Then, through the rapid cooling of the pure water environment, resulting in the martensitic structure; however, the presence of a large number of metal ions leads to a decrease in the speed of heat conduction and absorption of some heat.

Compared to the surrounding matrix area, the micropores occupy a smaller region, and the solutions inside and outside the pores are difficult to disperse, resulting in a concentration difference, a growth of the current density at the bottom of the hole, and a decrease in the pH value. Compared with the pure water, 3.5% NaCl solution contains more free ions and its local current density is higher; hence, the corresponding corrosion resistance is worse. As the cavitation time rises, the resulting passivation area of the sample gradually disappears.

Author Contributions: Conceptualization, L.L.; methodology, L.L. and L.Z.; formal analysis, L.L. and C.H.; writing—original draft preparation, J.M. and H.G.; writing—review and editing, L.L. and P.Y. All authors have read and agreed to the published version of the manuscript.

Funding: This research was funded by Xuzhou Science and Technology Program (KC21002), Natural Science Foundation of the Jiangsu Higher Education Institutions of China (23KJA460013), and Jiangsu Natural Science Foundation (BK20180177).

Institutional Review Board Statement: Not applicable.

Informed Consent Statement: Not applicable.

Data Availability Statement: No new data were created.

Acknowledgments: This work is supported by Xuzhou Science and Technology Program (KC21002), Natural Science Foundation of the Jiangsu Higher Education Institutions of China (23KJA460013), and Jiangsu Natural Science Foundation (BK20180177).

Conflicts of Interest: The authors declare no conflict of interest.

References

1. Yang, H.Y.; Zhou, H.; Lu, Y.X. Research status and development trend water hydraulic technology. *China Mech. Eng.* **2000**, *12*, 120–123+10.
2. Wu, Z.H.; Liu, X.M.; Li, B.B.; Zhao, Q.; Zhang, C.; Xie, Y.W.; Peng, J.J. Research on Cavitation Distribution Characteristics in Regulate Valve Based on Image Gray Statistics. *J. Mech. Eng.* **2023**, *59*, 307–316.
3. Suslick, K.S.; Flannigan, D.J. Inside a collapsing bubble: Sonoluminescence and the conditions during cavitation. *Annu. Rev. Phys. Chem.* **2008**, *59*, 659–683. [[CrossRef](#)] [[PubMed](#)]
4. Liu, Z.; Liu, Y.M.; Lu, L.; Sun, B. Cavitation Surge Numerical Simulation of Surface-sealed Structure of Poppet Valves. *Chin. Hydraul. Pneum.* **2022**, *46*, 72–81.
5. Ning, Q.; Han, Z.; Wenjie, Z.; Zhongyong, P.; Shouqi, Y.; Xiang, L. Investigation on Shock Wave Propagation and Impact of Cloud Cavitation Shedding. *J. Agric. Mach.* **2021**, *52*, 135–143.
6. Ma, C.; Shi, D.; Chen, Y.; Cui, X.; Wang, M. Experimental research on the influence of different curved rigid boundaries on electric spark bubbles. *Materials* **2020**, *13*, 3941. [[CrossRef](#)] [[PubMed](#)]
7. Wei, A.-b.; Gao, R.; Zhang, W.; Wang, S.-h.; Zhou, R.; Zhang, X.-b. Computational fluid dynamics analysis on flow-induced vibration of a cryogenic poppet valve in consideration of cavitation effect. *J. Zhejiang Univ. Sci. A Appl. Phys. Eng.* **2022**, *23*, 83–101. [[CrossRef](#)]
8. Chen, W. Cavitation Corrosion Performance of Several Oceaneering Metals. *Hot Work. Technol.* **2015**, *44*, 17–20.
9. Sreedhar, B.K.; Albert, S.K.; Pandit, A.B. Cavitation damage: Theory and measurements—A review. *Wear* **2017**, *372–373*, 177–196. [[CrossRef](#)]
10. Lei, C.Q.; Yuan, S.; Lin, N.M.; Wu, Y.C.; Fu, L.; Ma, G.S. Research Progress on Cavitation Erosion Damage and Protection of Titanium Alloy. *Surf. Technol.* **2022**, *51*, 128–142.
11. Wei, M.J.; Chen, L.; Wu, T.; Hong-Yan, Z.; Hai-Hang, C. Mechanism of the motion of spherical microparticle induced by a collapsed microbubble. *Acta Phys. Sin.* **2017**, *66*, 167–175.
12. Hutli, E.; Fekete, T.; Nedeljkovic, M. Surface characteristics and cavitation damage progress in ductile materials. *Eng. Fail. Anal.* **2019**, *106*, 104157. [[CrossRef](#)]
13. Tong, Z.P.; Jiao, J.F.; Zhou, W.F.; Yang, Y.C.; Liu, H.; Sun, Y.; Ren, X. Improvement in cavitation erosion resistance of AA5083 Aluminium alloy by laser shock processing. *Surf. Coat. Technol.* **2019**, *377*, 124799. [[CrossRef](#)]
14. Qin, Z.; Bremhorst, K.; Alehossein, H.; Meyer, T. Simulation of cavitation bubbles in a convergent-divergent nozzle water jet. *J. Fluid Mech.* **2007**, *573*, 1–25. [[CrossRef](#)]
15. Yang, Y.; Shan, M.; Kan, X.; Shangguan, Y.; Han, Q. Thermodynamic of collapsing cavitation bubble investigated by pseudopotential and thermal MRT-LBM. *Ultrason. Sonochem.* **2019**, *62*, 104873. [[CrossRef](#)] [[PubMed](#)]
16. Shang, M.L.; Yang, Y.; Qiu, C.L.; Shu, F.Y.; Han, Q.B. Numerical study of cavitation bubble collapse dynamics near a curved wall by the volume of fluid method. *J. Appl. Acoust.* **2022**, *41*, 548–557.
17. Shi, S.G.; Wang, G.Y. Thermal effect on cavitation in different fluids. *J. Ship* **2021**, *25*, 263–272.
18. Graat, P.C.J.; Somers, M.A.J. Simultaneous Determination of Composition and Thickness of Thin IronOxide Films from XPS Fe 2p Spectra. *Appl. Surf. Sci.* **1996**, *100–101*, 36–40. [[CrossRef](#)]
19. Alexander, V.; Naumkin, A.K.-V.; Stephen, W.G.; Cedric, J.P. NIST X-ray Photoelectron Spectroscopy Database. 2012. Available online: <https://srdata.nist.gov/xps/Default.aspx> (accessed on 30 July 2023).
20. Lin, C.; Zhao, X.B.; Zhang, Y.F. Research Progress on Cavitation-corrosion of Metallic Materials. *J. Chin. Soc. Corros. Prot.* **2016**, *1*, 11–19.

Disclaimer/Publisher’s Note: The statements, opinions and data contained in all publications are solely those of the individual author(s) and contributor(s) and not of MDPI and/or the editor(s). MDPI and/or the editor(s) disclaim responsibility for any injury to people or property resulting from any ideas, methods, instructions or products referred to in the content.